COMMUNICATION

Size effect of TiO_2 nanoparticles on the printable mesoscopic perovskite solar cell

Ying Yang, Kwangho Ri, Anyi Mei, Lingfeng Liu, Min Hu, Tongfa Liu, Xiong Li, Hongwei Han*

The size effect of TiO_2 photoanode has been investigated on the hole-conductor-free fully printable mesoscopic perovskite solar cells based on carbon counter electrode and (5-$AVA)_x(MA)_{1-x}PbI_3$ perovskite. With the optimized diameter of 25 nm TiO_2 nanoparticles, a champion device exhibits an efficiency of 13.41%.

Due to the exhaustion of fossil fuels and aggravation of environmental pollution problems, the development of clean and renewable energy is becoming more and more urgent. Solar energy is considered as the most promising source of renewable energy due to its abundance and availability. Although planar junction devices, usually made of silicon, have dominated the commercial market over the past decades, these photovoltaic technologies still have constraints in market development on account of both the expensive materials and the complex manufacturing processes[1, 2]. Realizing the full potential of the vast solar energy market requires a new generation of photovoltaic devices that are both efficient and low-cost, mesoscopic solar cells have become the object of ongoing investigation. Different from traditional silicon solar cells, the charge separation and transferring of mesoscopic solar cells take place in two different materials[3], allowing adequate space for the development of novel materials to improving the performance of the device.

As the key component of mesoscopic solar cells, mesoporous films based on wide band gap semiconductor materials have attracted more and more interest owing to their fascinating properties such as tunable pore sizes, high surface areas, controllable framework compositions, and stable characteristics, as well as their wide promising applications[4-7]. Its multifarious morphologies such as nanoparticles[8, 9], nanowires[10, 11], nanosheets[12], nanotubes[13, 14], spheres[15, 16] and some other mesoscopic structures[17-21] are widely used in dye-sensitized solar cells, one of typical mesoscopic solar cells. Up to now, a high certified efficiency of 11.9% has been obtained in dye-sensitized solar cells based on the TiO_2 nanocrystalline mesoscopic structure and liquid electrolyte.[22]

Stemming from dye-sensitized solar cells, organometal trihalide perovskite solar cells, pioneered by Miyasaka and coworkers[23], have emerged as a promising technology with a mesoscopic structure in past two years. Normally, these perovskite based mesoscopic solar cells are composed of a mesoscopic layer such as TiO_2 as an electron collector, an organometal trihalide perovskite such as $CH_3NH_3PbI_3$ as a light absorber, a hole transport material (HTM) such as spiro-OMeTAD as a electronic block layer and a noble metal film such as Au as a counter electrode. Presently, a high certificated efficiency up to 20.1% was obtained.[24] Indeed, the HTM of spiro-OMeTAD and noble counter electrode of Au in the device are so expensive and will be a great obstacle for future commercial applications.

In our group, we have developed a hole-conductor-free mesoscopic perovskite solar cell, in which the mesoscopic TiO_2 layer, ZrO_2 layer and carbon counter electrode layer are printed layer by layer and the perovskite are dropping into the trilayer mesoscopic films. This design combines the low-cost of mesoscopic solar cells, the continuous production process and promises extensive application prospect. A high certified efficiency up to 12.84% and long stabilization were obtained with (5-$AVA)_x(MA)_{1-x}PbI_3$ based mesoscopic solar cells[25]. However, as the key component of mesoscopic solar cells, the size effect of TiO_2 nanoparticles on the mesoscopic perovskite solar cells is very important to the characterization of devices, there is no paper reported about it in perovskite based solar cell. In this work, the TiO_2 nanoparticles with different size have been synthesized and the size effect on the mesoscopic perovskite solar cell is investigated. With the optimized TiO_2 nanoparticles of 25nm, a maximum efficiency of 13.41% was achieved in the hole-conductor-free, fully printable mesoscopic perovskite solar cells with carbon counter electrode.

Figure 1 shows the transmission electron microscopy (TEM) images of different sized TiO_2 nanoparticles prepared by a simple hydrothermal method. It could be found that the size of the nanoparticles ranges from several to several tens nanometers. The size of TiO_2 nanoparticles in the samples (a), (b), (c) and (d) were calculated from the average values of a set of at least twenty samples. X-ray diffraction (XRD) patterns of TiO_2 nanoparticles with different size are presented in Figure S1. The peaks at 25.26º, 37.77º, 48.00º, 53.86º, 54.98º, 62.65º are corresponding to (101), (004), (200), (105), (211) and (204), which are in good agreement with the standard anatase TiO_2 crystal structure. The particle size is calculated using the Debye-Scherer's law,

$$D = K\lambda/\beta\cos\theta$$

where D is the particle diameter, K is a constant, λ is the wavelength of Cu Kα radiation, β is the full width at half-maximum (FWHM) in radians, and θ is the scattering angle. According to the FWHM of the strongest (101) diffraction peak, the estimated particle diameters for the four kinds of TiO$_2$ nanoparticles are about 15 nm, 20 nm, 25 nm and 30 nm, respectively. These results are in good agreement with the size determination of the TiO$_2$ nanoparticles derived from TEM. As shown in the Table 1, the BET specific surface area of 15 nm nanoparticles is 139.8 m^2/g, which has pore size of 14.7 nm and porosity as high as 66.8%. With the increase of the size of TiO$_2$ nanoparticles, the pore size is increased simultaneously, but the specific surface area and the porosity decreased. When the particle size is 30 nm, the specific surface area and the porosity present the smallest value of 59.6 m^2/g and 60.1%, respectively.
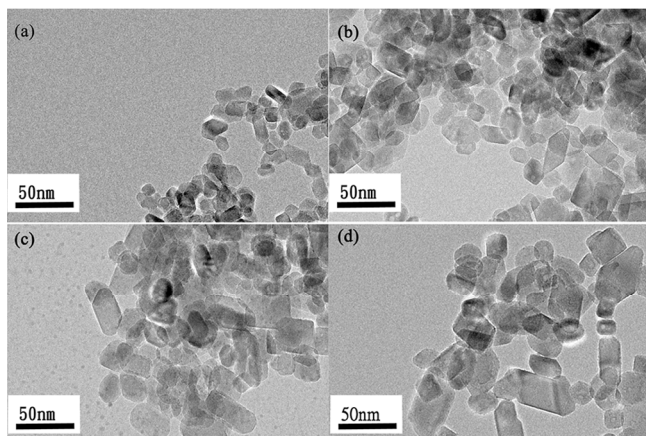

Figure 1. TEM patterns of different sized TiO$_2$ nanoparticles.
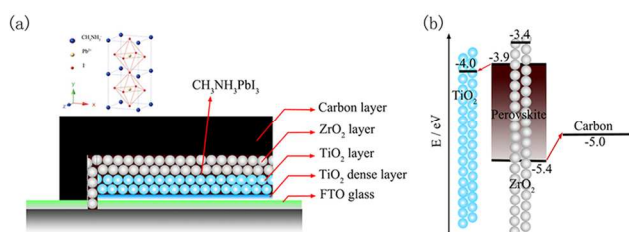

Figure 2. a) A schematic structure of carbon electrode based mesoscopic perovskite solar cell device. b) The corresponding energy level of TiO$_2$, perovskite, ZrO$_2$ and carbon.

Table 1. Characterization of synthesized TiO$_2$ nanoparticles.

TiO$_2$ samples	Surface Area (m^{2}g^{-1})	Pore Size (nm)	Pore Volume (cm^3/g)	Porosity
15nm TiO$_2$ NP	139.8	14.7	0.515	66.8%
20nm TiO$_2$ NP	111.1	18.7	0.520	67.0%
25nm TiO$_2$ NP	79.5	25.8	0.515	66.8%
30nm TiO$_2$ NP	59.6	25.8	0.385	60.1%

Figure 2a shows a schematic structure of the carbon electrode based mesoscopic perovskite solar cell. A typical sandwich structure composed of a mesoscopic TiO$_2$ nanocrystalline layer, a mesoscopic ZrO$_2$ spacer layer and a mesoscopic carbon layer, is constructed on a FTO glass substrate with a full printing technology. The cross-sectional image of the fully printable mesoscopic perovskite solar cell is presented in Figure S2, which indicates that a 0.95 μm TiO$_2$

nanocrystalline layer, a 1.65 μm ZrO$_2$ insulating layer and a 13.05 μm carbon layer are layered on the FTO glass, and the perovskite are filled in the triple mesoscopic layers. The corresponding energy levels of TiO$_2$, perovskite, ZrO$_2$ and carbon are illustrated in Figure 2b. Energy levels are expressed in electron volts (eV) using vacuum level as a reference. The conduction band edges of TiO$_2$, ZrO$_2$, and MAPbI$_3$ are at -4.0, -3.4 and -3.9 eV, respectively, while the valence band edge of the MAPbI$_3$ is at -5.4 eV and the Fermi level of carbon at -5.0 eV. The photo-generated electron-hole pairs are separated by injecting electrons into TiO$_2$ and transporting holes to the carbon and then forming photocurrent in the device. Since there is an offset of 0.6 eV between the conduction band of TiO$_2$ and that of ZrO$_2$, the electrons on perovskite conduction band could only be injected into TiO$_2$. In addition, the TiO$_2$ compact layer deposited on the FTO glass substrates block holes on the valence band of perovskite.

Photoanodes based on different sized TiO$_2$ nanoparticles were used to investigate the size effect on the performance of hole-conductor-free, fully printable mesoscopic perovskite solar cells. After assembling the mesoscopic perovskite solar cell with different sized TiO$_2$ nanoparticles, four key parameters of short-circuit photocurrent density (J_{sc}), open-circuit photovoltaic (V_{oc}), fill factor (FF) and power conversion efficiency (η) are summarized in Figure S3, where each data set is carried out from at least ten mesoscopic perovskite solar cells. It could be found that the J_{sc} of the devices with 20 nm sized TiO$_2$ have a maximum value. As the diameter of the particles increases from 15 nm to 20 nm, the J_{sc} increases from 21.1 mA/cm^2 to 23.3 mA/cm^2. Because of the narrow tunnels in 15 nm TiO$_2$ mesoscopic framework, the perovskite cannot penetrate into the bottom of the TiO$_2$ layer easily. When the TiO$_2$ nanoparticles increase to 20 nm, the improved pore filling caused by the larger pores size lead an improvement of the J_{sc}. However, with the size further increasing to 30nm, the J_{sc} presents a little bit lower value, which may be ascribed to the reduction of the porosity. Since the reduction of porosity means the less filling amounts of perovskite in the mesoscopic TiO$_2$ framework and this would ultimately results in a reduction of J_{sc}. As shown in Figure S3c, the FF increases from 0.52 to 0.61, the reason may be attributed to the reduction in electron transport resistance of the TiO$_2$ mesoscopic structure and the better filling of the perovskite solution, which are both caused by the further increased size of the TiO$_2$ nanoparticles. As a result of a compromise between V_{oc}, J_{sc} and the FF, the maximum of the average power conversion efficiency of about 11.31% was achieved when the TiO$_2$ nanoparticles were 25 nm. Figure S4 presents the J-V curve of a champion device of hole-conductor-free, fully printable mesoscopic perovskite solar cell, which is based on 25 nm TiO$_2$ nanoparticles and indicates an efficiency of 13.41% with J_{sc} of 22.93 mA/cm^2, V_{oc} of 0.867 V and FF of 0.67.

In order to extract quantitative information on the yield of light-induced charge separation, we performed time-resolved photoluminescence (PL) decay measurements on the (5-AVA)$_x$(MA)$_{1-x}$PbI$_3$ perovskite-filled TiO$_2$ mesoscopic films with four different sized TiO$_2$ nanoparticles respectively, which are presented in Figure 3. With global biexponential fits, the PL decay of the (5-AVA)$_x$(MA)$_{1-x}$PbI$_3$ perovskite contained in 15 nm, 20 nm, 25 nm and 30 nm sized TiO$_2$ films exhibits a time-constant of τ_1 = 7.43 ns, 4.73 ns, 3.36 ns and 2.13 ns respectively, which means that with the increasing diameter of the TiO$_2$ nanoparticles from 15 nm to 30 nm, the rate of the electron injection from perovskite into TiO$_2$ becomes faster, resulting in a higher electron injection quantum efficiency after the electron-hole separation. This could be attributed to the better filling of the (5-AVA)$_x$(MA)$_{1-x}$PbI$_3$ perovskite within the mesoscopic TiO$_2$ films and the more complete contact between the TiO$_2$ and the perovskite as the TiO$_2$ size increased.
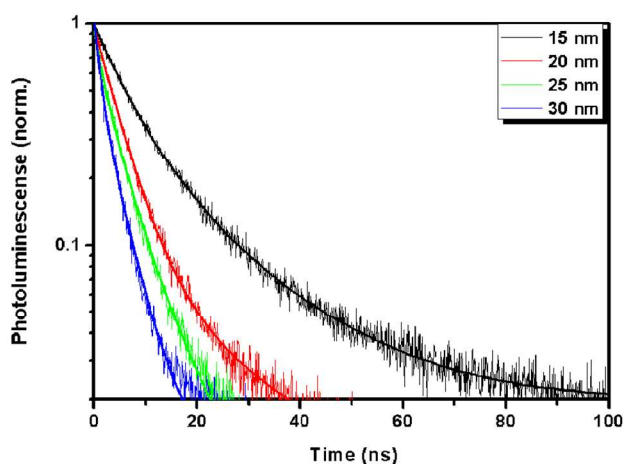
Figure 3. Normalized time-resolved photoluminescence intensity of different sized TiO_2/perovskite films.
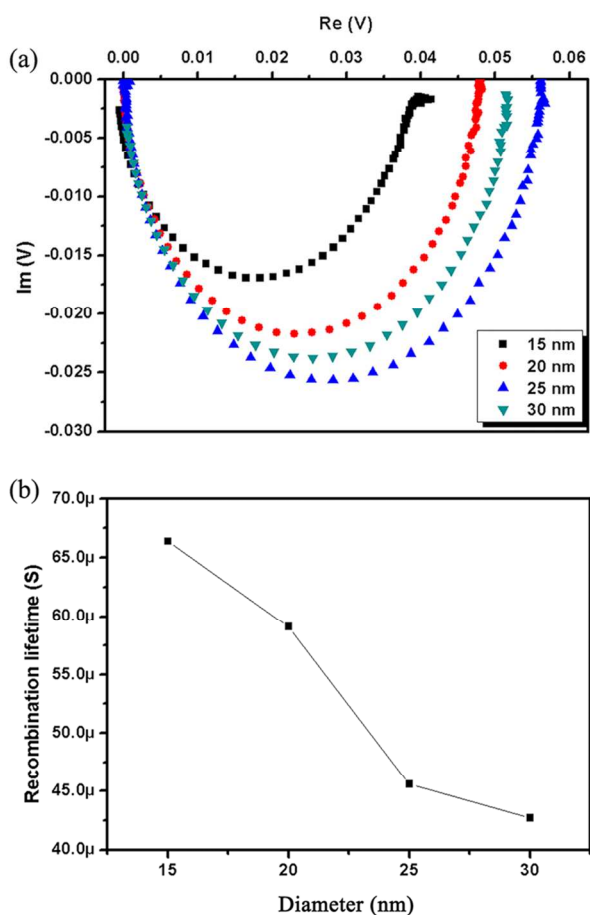

Figure 4. a) IMVS plots of carbon electrode based mesoscopic perovskite solar cells with different sized TiO_2 nanoparticles under 0.1 mW/cm² illuminations. b) The effects of different sized TiO_2 nanoparticles on recombination lifetime.

The charge transport mechanism within the nanocrystalline semiconductor films of the photoanode could be detected by the intensity modulated photocurrent spectroscopy (IMPS) measurement.

Figure S5 presents the IMPS curves of the photoanode of different sized TiO_2 nanoparticles. The transport time τ_d of the injected electrons through the TiO_2 film can be calculated from the equation

$$\tau_d = \frac{1}{2\pi f_{d,\ min}}$$

where $f_{d,\ min}$ is the characteristic frequency at the minimum of the IMPS imaginary component. The simulation results show that τ_d values are estimated to be 2.1×10^{-6} s, 1.209×10^{-6} s, 1.160×10^{-6} s and 1.104×10^{-6} s in the devices with the TiO_2 nanoparticles of 15 nm, 20 nm, 25 nm and 30 nm, respectively. In addition, the electron diffusion coefficient D_n could be calculated from the equation

$$D_n = \frac{d^2}{2.35\tau_d}$$

where d is the thickness of the photoanode. Therefore, the D_n in the TiO_2 films with the thickness of 0.95 µm with the TiO_2 nanoparticles of 15 nm, 20 nm, 25 nm and 30 nm are calculated to be 1.83×10^{-3}, 3.20×10^{-3}, 3.31×10^{-3} and 3.48×10^{-3} cm²·s⁻¹ respectively. It is clear that the charge transport within the film based on larger TiO_2 nanoparticles is faster than that of the smaller TiO_2 nanoparticles, which suggests that the charge collection efficiency of mesoscopic solar cell could be improved by larger sized TiO_2 nanoparticles.

The characterization of the charge transport and electron–hole recombination in mesoscopic perovskite solar cell, of which the TiO_2 layer was composed of different sized TiO_2 nanoparticles, were obtained by the intensity modulated photovoltage spectroscopy (IMVS) measurement. Figure 4a shows the typical Nyquist plots of IMVS characterization. The electron lifetime τ_n is measured as a function of photovoltage, calculated using the equation

$$\tau_n = \frac{1}{2\pi f_{n,min}}$$

where $f_{n,\ min}$ is the frequency of the minimum of the semicircle in the IMVS plots. In general, the longer lifetime of excited electron indicates a slower recombination rate and the higher conduction band electron density, which is related to the higher value of V_{oc}.[26] The values of electron lifetime τ_n are presented in Figure 4b, which are estimated to be 6.64×10^{-5} s, 5.91×10^{-5} s, 4.56×10^{-5} s and 4.27×10^{-5} s for the devices preparing from 15 nm, 20 nm, 25 nm and 30 nm sized TiO_2 particles respectively. This indicates that the electron lifetime in the perovskite solar cell decreases with the size increase of TiO_2 nanoparticles.

The kinetics characterization of charge transfer at the interface between the perovskite and mesoscopic TiO_2 of devices based on different sized TiO_2 nanoparticles was carried out with electrochemical impedance spectra (EIS) analysis, which was collected in a frequency range from 0.1 Hz to 1 MHz at -0.7 V under dark condition. Figure 5 presents the Nyquist plot, where an obvious semicircle at low frequency and a much smaller arc at high frequency (in the inset) are observed in the measured frequency range. The smaller arc at high frequency is assigned to the charge transfer/transport resistance (R_{sc}) due to the selective contact or the interface, and the arc at low frequency is assigned to the interfacial and/or bulk recombination, R_{rec}.[27, 28] The inset presents the first semicircle at high frequency with high magnification, which shows similar semicircle and indicates the devices based different sized TiO_2 nanoparticles have similar R_{sc}, The beginning x-intercept of the curve, corresponding to a series resistance, decreases with the size increase of TiO_2 nanoparticles, which agrees well with the result of the IMPS in Figure S5. Meanwhile, at low frequency the device based on 15nm TiO_2 nanoparticles shows the largest arc, indicating the R_{rec} of the device is the highest among these four kinds of solar

cells. It also could be found that with the size increase of TiO$_2$ nanoparticles, the R$_{rec}$ becomes smaller and the device based on 30nm sized TiO$_2$ nanoparticles presents the smallest value. This could be attributed to the electronic contact between the TiO$_2$ and the Carbon electrode, which increases recombination of electrons and holes. This also certifies that the device with increased TiO$_2$ size presents a lower V_{oc} and J_{sc}.
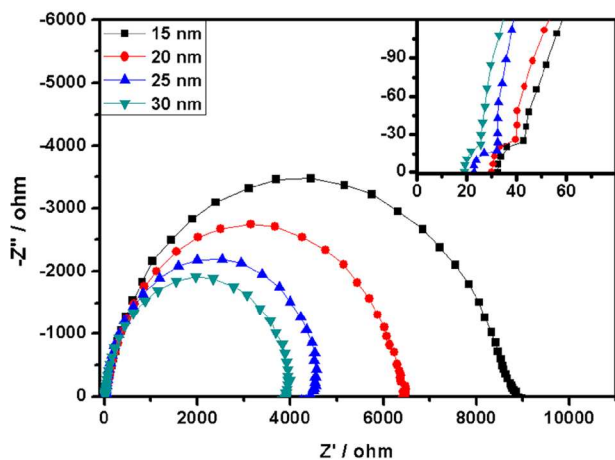

Figure 5. EIS plots of carbon electrode based mesoscopic perovskite solar cells with different sized TiO$_2$ nanoparticles.

Conclusions

In summary, different sized TiO$_2$ nanoparticles was synthesized with hydrothermal method and applied as an electron collector on the hole-conductor-free fully printable mesoscopic perovskite solar cells based on carbon counter electrode and (5-AVA)$_x$(MA)$_{1-x}$PbI$_3$ perovskite materials. The size effect of TiO$_2$ nanoparticles on the carbon counter electrode based mesoscopic perovskite solar cells was investigated. Results indicate that the size of TiO$_2$ particles not only affects the infiltration of precursor and the contact between perovskite crystal and TiO$_2$, but also significantly influences the charge transfer kinetics at the perovskite/TiO$_2$ interface. With the optimized diameter of 25 nm TiO$_2$ nanoparticles, the carbon counter electrode based perovskite mesoscopic solar cell exhibits a best power conversion efficiency of 13.41% in ambient air under simulated standard AM 1.5 condition.

Acknowledgements

Notes and references

Michael Grätzel Center for Mesoscopic Solar cells, Wuhan National Laboratory for Optoelectronics. School of Optical and Electronic Information, Huazhong University of Science and Technology, Wuhan, Hubei, P. R. China, 430074. E-mail: hongwei.han@mail.hust.edu.cn; Tel: +86 27 8779 3027

Electronic Supplementary Information (ESI) available:

Experimental section, XRD pattern of nanoparticles, cross-section SEM of device, Size effects on the key photovoltaic performance parameters and IMPS of the devices.

1 M. Grätzel, R. A. Janssen, D. B. Mitzi and E. H. Sargent, *Nature*, 2012, 488, 304-312.
2 Z. L. Ku, Y. G. Rong, M. Xu, T. F. Liu and H. W. Han, *Scientific Reports*, 2013, 3, 5.
3 C. Grätzel and S. M. Zakeeruddin, *Materials Today*, 2013, 16, 11-18.
4 Z.-S. Wang, H. Kawauchi, T. Kashima and H. Arakawa, *Coordination chemistry reviews*, 2004, 248, 1381-1389.
5 W. Li, Q. Yue, Y. Deng and D. Zhao, *Adv. Mater.*, 2013, 25, 5129-5152.
6 J. H. Shin and J. H. Moon, *Langmuir*, 2011, 27, 6311-6315.
7 W. Li, Z. Wu, J. Wang, A. A. Elzatahry and D. Zhao, *Chemistry of Materials*, 2014, 26, 287-298.
8 S. Nakade, Y. Saito, W. Kubo, T. Kitamura, Y. Wada and S. Yanagida, *The Journal of Physical Chemistry B*, 2003, 107, 8607-8611.
9 J. G. Yu, J. J. Fan and K. L. Lv, *Nanoscale*, 2010, 2, 2144-2149.
10 X. J. Feng, K. Shankar, O. K. Varghese, M. Paulose, T. J. Latempa and C. A. Grimes, *Nano lett.*, 2008, 8, 3781-3786.
11 M. L. Sun, W. Y. Fu, H. B. Yang, Y. M. Sui, B. Zhao, G. C. Yin, Q. Li, H. Zhao and G. T. Zou, *Electrochem. Commun.*, 2011, 13, 1324-1327.
12 K. L. Lv, Q. J. Xiang and J. G. Yu, *Applied Catalysis B-Environmental*, 2011, 104, 275-281.
13 G. K. Mor, K. Shankar, M. Paulose, O. K. Varghese and C. A. Grimes, *Nano lett.*, 2006, 6, 215-218.
14 M. Guo, K. Y. Xie, J. Lin, Z. H. Yong, C. T. Yip, L. M. Zhou, Y. Wang and H. T. Huang, *Energy Environ. Sci.*, 2012, 5, 9881-9888.
15 J. G. Yu, J. J. Fan and L. Zhao, *Electrochimica Acta*, 2010, 55, 597-602.
16 P. Xiang, X. Li, H. Wang, G. Liu, T. Shu, Z. Zhou, Z. Ku, Y. Rong, M. Xu, L. Liu, M. Hu, Y. Yang, W. Chen, T. Liu, M. Zhang and H. Han, *Nanoscale research letters*, 2011, 6, 606.
17 B. Cheng, Y. Le and J. G. Yu, *Journal Of Hazardous Materials*, 2010, 177, 971-977.
18 P. L. Hung, M. H. Wen, K. H. Hung, J. S. Bow, H. W. Wang, J. C. C. Han, Y. F. Lu, J. C. Chung, Y. C. Liu, Y. Z. Zeng and K. R. Ratinac, *J. Chin. Chem. Soc.*, 2010, 57, 1157-1161.
19 M. Jin, S. S. Kim, M. Yoon, Z. Li, Y. Y. Lee and J. M. Kim, *Journal of Nanoscience and Nanotechnology*, 2012, 12, 815-821.
20 J. S. King, E. Graugnard and C. J. Summers, *Adv. Mater.*, 2005, 17, 1010-1013.
21 S. J. Stott, R. J. Mortimer, S. E. Dann, M. Oyama and F. Marken, *Phys. Chem. Chem. Phys.*, 2006, 8, 5437-5443.
22 A. Yella, H. W. Lee, H. N. Tsao, C. Yi, A. K. Chandiran, M. K. Nazeeruddin, E. W. Diau, C. Y. Yeh, S. M. Zakeeruddin and M. Gratzel, *Science*, 2011, 334, 629-634.
23 A. Kojima, K. Teshima, Y. Shirai and T. Miyasaka, *J. Am. Chem. Soc.*, 2009, 131, 6050-+.
24 http://www.nrel.gov/ncpv/images/efficiency_chart.jpg
25 A. Mei, X. Li, L. Liu, Z. Ku, T. Liu, Y. Rong, M. Xu, M. Hu, J. Chen, Y. Yang, M. Gratzel and H. Han, *Science*, 2014, 345, 295-298.
26 M. Xu, G. Liu, X. Li, H. Wang, Y. Rong, Z. Ku, M. Hu, Y. Yang, L. Liu, T. Liu, J. Chen and H. Han, *Org. Electron.*, 2013, 14, 628-634.
27 M. Hu, L. Liu, A. Mei, Y. Yang, T. Liu and H. Han, *J. Mater. Chem. A*, 2014, 2, 17115-17121.
28 A. Dualeh, T. Moehl, N. Tetreault, J. Teuscher, P. Gao, M. K. Nazeeruddin and M. Grätzel, *ACS Nano*, 2013.